Modifying the Adsorption Characteristic of Inert Silica Films by Inserting Anchoring Sites

Stefan Ulrich, Niklas Nilius,[*] and Hans-Joachim Freund

Fritz-Haber-Institut der MPG Berlin, Berlin, Germany

Umberto Martinez, Livia Giordano, and Gianfranco Pacchioni[†]

Dipartimento di Scienza dei Materiali, Università di Milano-Bicocca, Milano, Italy
(Received 14 August 2008; published 8 January 2009)

The adsorption properties of thin silica films on Mo(112) have been tailored by embedding single Pd atoms into the nanopores of the oxide material. The embedded Pd is able to anchor metal adatoms that would not bind to the inert silica surface otherwise. Several adsorption structures, e.g., Pd-Pd, Ag-Pd, and Au-Pd complexes, have been prepared in this way and analyzed with the STM and density functional theory. The binding strength of the different adatoms to the surface is determined by the number of electrons in their frontier orbitals, which introduce a repulsive interaction with the oxide electronic states and weaken the covalent bond to the Pd anchor.

Tailoring the adsorption properties of solid materials has been a long-term objective in surface science [1–3]. The functionalization of surfaces is determined by several aspects. First, the density and spatial arrangement of binding sites need to be controlled. Second, the adsorption behavior should be chemically selective, admitting only certain species to interact with the surface. And last, the internal structure of the ad-material should be tunable. Systems with designable adsorption properties have a wide range of applications, e.g., as catalysts in stereoselective reactions, chemical sensors, and template surfaces for self-organization processes.

Several approaches have been developed to fabricate tunable adsorption systems; however, most of them are unable to fulfill all the specifications mentioned above. Regular arrays of binding sites are produced on vicinal surfaces [4], molecular template structures [5], and epitaxial systems exhibiting an ordered network of dislocations [6,7]. Chemical sensitivity is achieved by equipping the surface with suitable functional groups to stimulate binding to the desired adsorbates. Alternatively, the size-selective adsorption behavior of porous materials, e.g., zeolites, is exploited to tune surface reactions via the adsorbate diameter [1,8]. Controlling the internal structure of the ad-material remains the most difficult part. Here, mainly atomic manipulation with the scanning tunneling microscope (STM) has been employed to assemble aggregates with a defined structure and chemical composition [9,10].

In this Letter, we report a new approach towards a functionalized adsorption system that is based on the insertion of defined binding sites into an initially inert surface. A suitable system to realize this concept is a porous silica film prepared on Mo(112) [11,12]. The film is chemically inactive and only physisorbs inorganic molecules, like CO and H_2O [13]. However, small metal atoms can be inserted into the oxide nanopores [14], as demonstrated for Pd and Ag, whereas larger atoms such as Au are unable to penetrate the holes in the silica top layer [15,16]. The inserted atoms remain close to the surface and might be used to stabilize adsorbates on the inert oxide film.

The approach is similar to the doping of oxide materials with impurity atoms or point defects, as an alternative route to creating surface binding sites. Substantial changes in the adsorption behavior were indeed reported for Li- or Ti-doped SiO_2, and MgO surfaces containing oxygen vacancies [14,17–19]. However, while doping affects the global electronic and chemical properties of the oxide material, the insertion of single-atom anchors modifies the binding characteristics only locally. The possibility of using Pd atoms incorporated into a silica film to anchor metal adatoms is now demonstrated with a STM and density functional theory (DFT), approving this new route towards a functionalized adsorption system.

The experiments are performed in a custom built UHV-STM operated at 10 K. The silica film is prepared on an oxygen precovered Mo(112) surface by depositing 1.2 monolayers silicon at 800 K in an O_2 ambience of 1×10^{-7} mbar [11,12]. Sample annealing to 1200 K leads to the formation of a crystalline SiO_2 layer, as indicated by the sharp $c(2 \times 2)$ LEED pattern [12]. The film is composed of a network of corner-sharing SiO_4 tetrahedrons, whereby every Si atom is connected via bridging O atoms to three Si neighbors in the plane and to the Mo surface underneath [Fig. 1(a), inset]. The resulting honeycomb structure consists of $-Si-O-$ hexagons enclosing a hole of 3–4 Å diameter that gives access to a nanopore at the Mo-SiO_2 interface. The main structural defects of the film are [$\bar{1}10$]-oriented domain boundaries, caused by the lateral displacement of two oxide patches by a Mo unit-cell
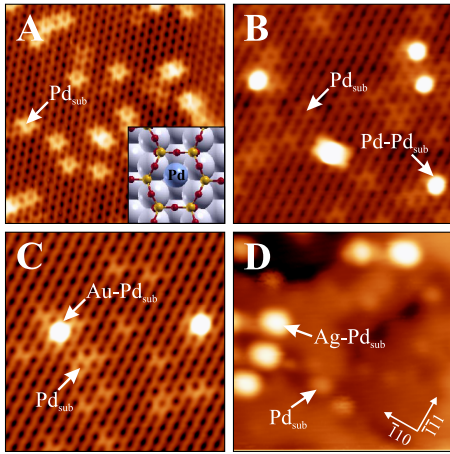
FIG. 1 (color online). (a) STM topographic image of
$SiO_2/Mo(112)$ after insertion of Pd_{sub} species ($U_s = 1.2$ V,
14×14 nm^2). (b) Same surface after deposition of single Pd
(0.5 V), (c) Au (0.5 V), and (d) Ag atoms (1.9 V, 14×14 nm^2).
While only Pd_{sub} species are observed in (a), new ad-structures
become visible in (b–d). The inset in (a) shows a structure model
of a Pd_{sub} in a silica pore (Si, small yellow; O, small red; and Mo,
large blue circles).

vector (Fig. 2, dashed arrows). Along such boundaries, the
regular hexagons are replaced by larger $-$Si$-$O$-$ octa-
gons alternating with $-$Si$-$O$-$ squares.

Single Pd, Ag, and Au atoms are deposited onto the film
from high-purity metal wires (99.95%) wrapped with a
tungsten filament. Although deposition is performed at
20 K, the atoms have sufficient initial energy to perform
transient diffusion into their equilibrium configuration.
The local density of states (LDOS) of the sample is probed
by differential conductance (dI/dV) spectroscopy per-
formed with lock-in technique and open feedback loop
(10 mV/1137 Hz modulation). DFT calculations are car-
ried out with the generalized gradient approximation using
the PW91 exchange-correlation functional and a plane
wave basis set (400 eV energy cutoff) as implemented in
the VASP code [20,21]. The electron-ion interaction is in-
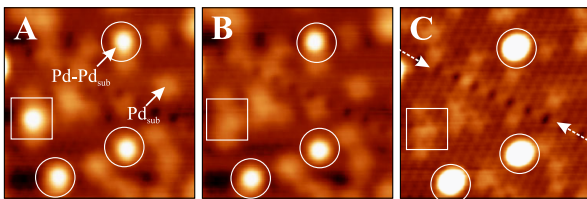cluded by the projector-augmented-waves method [22].

FIG. 2 (color online). (a) STM topographic image of Pd_{sub} and
Pd-Pd_{sub} species on $SiO_2/Mo(112)$ ($U_s = 1.0$ V, 10×10 nm^2).
(b) As in (a) but after controlled removal of the adatom marked
by the square box. (c) As in (b) but with enhanced contrast to
show the silica atomic structure. Below the removed atom, the
signature of a Pd_{sub} becomes visible that has initially anchored
the ad-species. The circles indicate other Pd-Pd_{sub} complexes as
guides for the eye; the dashed arrows mark a silica domain
boundary.

The Mo(112) substrate is described by seven Mo layers,
whereby the three bottom layers are kept frozen at bulk
positions during geometry optimization. The silica film is
modeled with (4×2) and (6×4) supercells, correspond-
ing to a stoichiometry of $Mo_{14}Si_2O_5$ and $Mo_{24}Si_6O_{15}$,
respectively.

STM topographic images of the bare film show the
characteristic honeycomb structure of the silica. Upon Pd
exposure, distinct hexagonal stars appear in images taken
at 0.5 V [Fig. 1(a)]. They transform into bright protrusions
of 0.7 Å height above 2.0 V sample bias. According to
earlier studies [16], the features are assigned to Pd atoms
that have penetrated the silica nanopores and bind to the
Mo-SiO$_2$ interface with 3.3 eV (referred to as Pd_{sub}). The
characteristic starlike contrast originates from a hybridiza-
tion between the Pd $5s$ and O $2p$ orbitals, which renders the
oxygen atoms of the hosting $-$Si$-$O$-$ ring visible in the
STM. Above $+2.0$ V sample bias, the Pd $5s$ becomes
directly accessible for tunneling electrons, and the contrast
localizes at the Pd_{sub} atom in the center of the pore [16].

To investigate the possibility of anchoring single
atoms to these Pd_{sub} species, three sets of experiments
are performed: (i) deposition of 1×10^{13} Pd atoms per
cm^2 onto a silica film already containing 2×10^{13} cm^{-2}
Pd_{sub} and deposition of (ii) 1×10^{12} cm^{-2} Au and
(iii) 1×10^{12} cm^{-2} Ag atoms onto a silica film with $1 \times
10^{13}$ cm^{-2} Pd_{sub} incorporated [Figs. 1(b)–1(d)]. In all three
cases, new species appear on the oxide surface, which
clearly differ in height, shape, and bias-dependent contrast
from the Pd_{sub} anchors. The species are imaged as round
protrusions at all sample biases, in contrast to the hexago-
nal shape of inserted Pd_{sub}, and reach apparent heights of
more than 2.0 Å (compared to 0.7 Å for Pd_{sub}). They are
not compatible with single Ag or Au atoms on the silica
surface, either. According to DFT calculations, both
atomic species only weakly interact with the oxide film
(adsorption energies below 0.05 eV) and perform rapid
diffusion even at low temperature [14,16]. Whereas the
Ag atom is able to pass the opening in the $-$Si$-$O$-$ hexa-
gons, producing similar STM features as the Pd_{sub}, the Au
atom is too big for penetration and binds exclusively at do-
main boundaries exposing larger pores. As the new species
are neither located along such boundaries nor exhibit the
unusual contrast of an embedded atom, they can safely be
discriminated from Ag and Au atoms. The adsorption
structures emerging after Pd, Ag, and Au deposition are
therefore assigned to single atoms bound to Pd_{sub} anchors
in the silica film, a hypothesis that will be supported by
further experimental evidence in the following.

The ad-species are easily removed from the oxide sur-
face by applying moderate voltage pulses to the STM tip
(3–5 V), as shown for a Pd-Pd_{sub} complex in Fig. 2. After
the manipulation experiment, the characteristic signature
of an embedded Pd_{sub} becomes visible in every case, sug-
gesting that the Pd_{sub} anchor is indeed required to stabilize
the adatom. Furthermore, the different ad-species exhibit
dI/dV fingerprints that clearly deviate from the spectro-

scopic response of the inserted atoms. For example, while a Pd_{sub} shows a weak dI/dV shoulder at $+2.3$ V, attributed to the Pd $5s$ orbital [16], a pronounced maximum at $+1.75$ V is observed for the Pd-Pd_{sub} complex [Fig. 3(a)]. Similarly, the Au-Pd_{sub} species exhibits enhanced dI/dV intensity at -0.2 V and $+1.6$ V (Fig. 4), whereas no maxima are revealed for Au monomers located at the domain boundaries. Only for Ag-Pd_{sub} complexes, no dI/dV spectra could be acquired, because the Ag atom easily desorbs during a spectroscopic run.

The attachment of Pd, Ag, and Au atoms to Pd_{sub} anchors in the silica film is verified by DFT calculations. In all three examples, the adatoms form covalent bonds with a Pd_{sub} sitting in an oxide pore, however, with rather different binding energies. The strongest interaction is found for Pd adatoms, which bind with 1.16 eV to the Pd_{sub} (bond length: 2.66 Å). Without a surface anchor, the binding strength decreases to 0.35 eV, and the atoms spontaneously penetrate the hole in the $-Si-O-$ hexagons. The adsorption energy of noble-metal atoms is considerably smaller and amounts to 0.35 eV for Au-Pd_{sub} and 0.19 eV for Ag-Pd_{sub} complexes (virtually no binding without Pd_{sub}). Surprisingly, the atom-atom bond lengths are with 2.54 Å for Au-Pd_{sub} and 2.85 Å for Ag-Pd_{sub} species not much different from the Pd-Pd_{sub} case and are even close to the values of the corresponding gas-phase dimers (Pd_2, 2.54 Å; Au-Pd, 2.68 Å). In contrast, the binding energy follows an opposite trend for gas-phase (Pd_2, 0.7 eV; Au-Pd, 1.4 eV) [23,24] and surface complexes.

The apparent contradiction between short interatomic distances and low binding energies of the different ad-structures indicates the presence of two competing interaction mechanisms on the silica surface. On the one hand, the adatoms form strong covalent bonds to the Pd_{sub} anchors. On the other hand, this attractive contribution is counterbalanced by the Pauli repulsion that is mainly exerted by the filled $2p$ states of the surface oxygen on the adatom. The repulsion is governed by the spatially most expanded adatom orbital, which is the $5s$ for Pd and Ag and
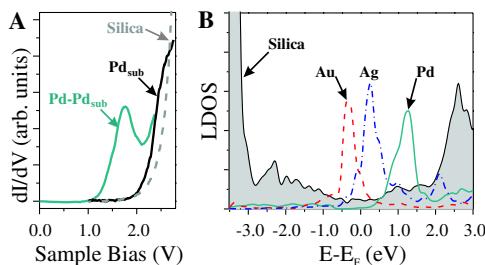
the $6s$ for the Au. Those frontier orbitals hybridize with the O $2p$ states upon adsorption, forming new states of antibonding character [Fig. 3(b)]. The strength of the repulsion and therefore the adatom-surface interaction is now controlled by the number of electrons in these hybrid states. The Pd $5s$-O $2p$ mixed state is located at $+1.25$ eV above the Fermi level (E_F) and therefore empty, which reduces the repulsion with the oxygen states and allows the formation of a strong Pd-Pd_{sub} bond. The binding energy is even higher than in gas-phase Pd_2, reflecting the stabilization effect of the Mo support. The position of the Pd $5s$-derived state above E_F manifests the charge neutrality of the adatom, as the state is empty in gas-phase Pd, too. The hybrid state shows up also experimentally and is assigned to the dI/dV peak at $+1.75$ V observed for Pd-Pd_{sub} complexes [Fig. 3(a)].

In contrast, the hybrid state formed between the Ag $5s$ (Au $6s$) orbital and the O $2p$ states is singly (doubly) occupied, as deduced from its calculated energy position at $+0.1$ eV (-0.3 eV) [Fig. 3(b)]. Because of the vicinity to E_F, they could not be identified in the dI/dV spectra, although the enhanced signal in conductance maps of Au-Pd_{sub} complexes at -0.2 V might indicate tunneling into the Au $6s$-O $2p$ state (Fig. 4). The electron(s) in the mixed metal-oxygen states induce substantial Pauli repulsion with the silica LDOS, which partly compensates the attractive interaction with the Pd_{sub} and gives rise to the small binding energies of Ag and Au atoms. The effect is larger for Au, because its valence s orbital is doubly occupied ($6s^2$ configuration) as a result of a charge transfer from the Mo support. The formation of anionic Au species has been observed for other oxide films before and manifests the strong electronegative character of gold [25,26]. Instead, the Ag adatom remains neutral on the silica sur-
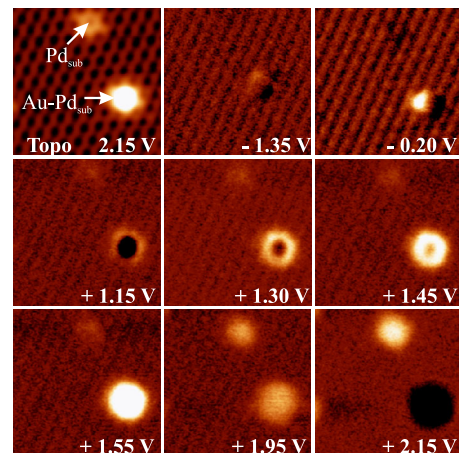

FIG. 4 (color online). Topographic image and dI/dV maps of a Pd_{sub} and a Au-Pd_{sub} species on SiO_2/Mo(112) taken at different sample biases (6×6 nm^2). The increase of the dI/dV signal at the Au-Pd_{sub} at -0.2 and $+1.55$ V marks two intrinsic states of the complex, whereas the ringlike enhancement at 1.0–1.5 V is related to a deformation of the silica lattice upon Au adsorption.

FIG. 3 (color online). (a) dI/dV spectra of a Pd_{sub}, a Pd-Pd_{sub} complex, and the bare silica surface (set point 2.5 V). (b) Calculated state density of the supported silica film (gray region). The line spectra depict the Pd $5s$ (solid line), Ag $5s$ (dash-dotted line), and Au $6s$ (dashed line) contribution to the hybrid state formed with the O $2p$ orbitals, when the respective adatom binds to a Pd_{sub} anchor.

face, since its 5s orbital carries a single electron as in gas-phase Ag. The comparable adsorption energies for Au and Ag atoms, in spite of different repulsive terms, reflect the balancing influence of the metal d states. Whereas the Au $5d$ states considerably strengthen the Au-Pd$_{sub}$ interaction, the Ag $4d$ is too low in energy to participate in the bond formation.

To reduce steric repulsion, the $-Si-O-$ hexagon hosting the Pd$_{sub}$ strongly relaxes upon adatom attachment. The effect is most pronounced for the Au-Pd$_{sub}$ complex due to the double occupancy of the Au $6s$-O $2p$ hybrid state. According to the DFT calculations, the opening in the $-Si-O-$ hexagon enlarges by several tenths of an angstrom ($\sim 5\%$) and enables the Au to approach the Pd$_{sub}$ anchor. As a result, the Au binding energy increases from 0.14 eV as calculated for a rigid geometry to 0.35 eV after structural relaxation. The ring widening is accompanied by a reduction of the silica LDOS next to the Au-Pd$_{sub}$ binding site, which reflects the decreasing Si-O orbital overlap in the enlarged hexagon. The reduced state density is indeed observed in dI/dV maps of the Au-Pd$_{sub}$ complex taken between 1.0 and 1.5 V sample bias (Fig. 4). To balance the outward relaxation of the hexagon, Si-O bonds need to be compressed in a circular region surrounding the adsorption site. The resulting increase of the oxide LDOS is also visible in dI/dV maps, and shows up as a ringlike intensity enhancement around the Au-Pd$_{sub}$ species. The ring diameter is approximated with 10 Å, indicating that mainly the next shell of $-Si-O-$ hexagons is affected by the compressive stress exerted by the enlarged silica pore. Similar ring structures are also observed for the Pd-Pd$_{sub}$ complexes.

In conclusion, Pd$_{sub}$ atoms incorporated into the nanopores of a thin silica film are able to anchor various adatoms at the originally inert oxide surface. The stabilization effect results from a strong covalent bonding between adatom and embedded Pd$_{sub}$, which is, however, partly compensated by the Pauli repulsion of the filled $2p$ states of the surface oxygen atoms. The strength of the repulsive interaction is dominated by the occupancy of the frontier orbitals of the different adatoms and increases when going from Pd with an empty valence s state, to neutral Ag and negatively charged Au species with singly and doubly occupied s orbitals, respectively. The ratio between repulsive and attractive terms in the anchoring process thus depends on the electronic properties of the adatoms, introducing a certain chemical sensitivity of the interaction mechanism. The approach described here can be employed to produce even more complex structures via subsequent attachment of different atomic species to the surface anchors. The successful insertion of single-atom binding sites into porous silica films on Mo(112) therefore presents a first step towards the preparation of a functionalized adsorption system.

*Corresponding author.
nilius@fhi-berlin.mpg.de
†Corresponding author.
gianfranco.pacchioni@unimib.it

[1] H. Li, M. Eddaoudi, M. O'Keeffe, and O. M. Yaghi, Nature (London) **402**, 276 (1999).
[2] *Functionalization of Nanomaterials*, edited by C. S. R. Kumar (Wiley-VCH, Weinheim, 2005).
[3] H. J. Freund, Surf. Sci. **601**, 1438 (2007).
[4] N. Neel, J. Kröger, and R. Berndt, Appl. Phys. Lett. **88**, 163 101 (2006).
[5] J. A. Theobald, N. S. Oxtoby, M. A. Phillips, N. R. Champness, and P. H. Beton, Nature (London) **424**, 1029 (2003).
[6] H. Brune, M. Giovannini, K. Bromann, and K. Kern, Nature (London) **394**, 451 (1998).
[7] C. Becker *et al.*, New J. Phys. **4**, 75 (2002).
[8] S. Bhatia, *Zeolite Catalysis: Principles and Applications* (CRC Press, Boca Raton, FL, 1990).
[9] N. Nilius, T. M. Wallis, and W. Ho, Science **297**, 1853 (2002).
[10] G. V. Nazin, X. H. Qui, and W. Ho, Science **302**, 77 (2003).
[11] T. Schroeder *et al.*, Surf. Rev. Lett. **7**, 7 (2000).
[12] J. Weissenrieder *et al.*, Phys. Rev. Lett. **95**, 076103 (2005).
[13] J. B. Giorgi, T. Schröder, M. Bäumer, and H.-J. Freund, Surf. Sci. Lett. **498**, L71 (2002).
[14] L. Giordano, A. Del Vitto, and G. Pacchioni, J. Chem. Phys. **124**, 034 701 (2006).
[15] M. Baron *et al.*, J. Phys. Chem. C **112**, 3405 (2008).
[16] S. Ulrich, N. Nilius, H.-J. Freund, U. Martinez, L. Giordano, and G. Pacchioni, Chem. Phys. Chem. **9**, 1367 (2008).
[17] J. X. Wang and J. H. Lunsford, J. Phys. Chem. **90**, 5883 (1986).
[18] M. C. Wu, C. M. Truong, and D. W. Goodman, Phys. Rev. B **46**, 12 688 (1992); B. K. Min, W. T. Wallace, and D. W. Goodman, J. Phys. Chem. B **108**, 14 609 (2004).
[19] M. Sterrer *et al.*, Angew. Chem., Int. Ed. **45**, 2630 (2006).
[20] J. P. Perdew *et al.*, Phys. Rev. B **46**, 6671 (1992).
[21] G. Kresse and J. Hafner, Phys. Rev. B **47**, 558 (1993); G. Kresse and J. Furthmüller, Phys. Rev. B **54**, 11 169 (1996).
[22] P. E. Blöchl, Phys. Rev. B **50**, 17 953 (1994).
[23] D. Andrea, U. Haussermann, M. Dolg, H. Stoll, and H. Preuss, Theor. Chim. Acta **78**, 247 (1991); P. Schwerdtfeger, Chem. Phys. Lett. **183**, 457 (1991); J. Ho, K. M. Ervin, M. L. Polak, M. K. Gilles, and W. C. Lineberger, J. Chem. Phys. **95**, 4845 (1991).
[24] *Handbook of Chemistry and Physics*, edited by D. R. Lide (CRC Press, Boca Raton, FL, 1998).
[25] M. Sterrer *et al.*, Phys. Rev. Lett. **98**, 096107 (2007).
[26] N. Nilius *et al.*, Phys. Rev. Lett. **100**, 096802 (2008).